From stars to quasars

Modeling radiation-dominated objects in astrophysics

Ivan Hubeny

NASA Goddard Space Flight Center, Greenbelt, MD 20771, USA

There is a whole class of astronomical objects for which radiation is not only a probe of the physical state, but is in fact an important energy balance agent. In these objects, radiative transfer plays a crucial role. Typical examples of such a situation are stellar atmospheres, interstellar matter and various structures within, and accretion disks, both around stellar mass degenerate objects (cataclysmic variables), and around supermassive black holes (quasars).

We concentrate on two objects – stellar atmospheres and quasar accretion disks, and show that since they have many similarities they can be modeled using an analogous approach. We will give a brief overview of recent progress in their modeling. On the stellar atmosphere side, very sophisticated non-LTE models including millions of lines are now being constructed. It is shown that they provide an excellent match to high-quality ground- and space-based spectra. In quasar modeling, we have constructed a grid of non-LTE disk models for a wide range of parameters, and begun a study of analysing observed data using the new models.

Keywords: stars: atmospheres—accretion disks—galaxies: active—radiative transfer

1 Introduction

An atmosphere of a star is generally any material connected physically to a star from which the photons escape to the surrounding space. In other words, it is a region where the radiation, observable by a distant observer, originates. What makes atmospheres of stars so special is the fact that because of the strong and energetic radiation field generated in stellar interiors, the radiation in an atmosphere is not merely a passive *probe* of the physical state of the atmosphere, but rather an important *energy balance agent.* In other words, radiation in fact *determines* the structure of the medium, yet the medium is probed *only* by this radiation. Another important feature is that photons have, under the typical conditions met in the stellar atmospheres, a much larger mean-free-path than massive particles. This means that radiation is able to transport information to large distances; in other words, radiation *couples* the physical states of rather distant regions of the atmosphere.

The other critical feature that follows from the presence of radiation-induced processes is that the medium is prone to departures from thermodynamic equilibrium. Indeed, the simple fact that we do *see* a star means that photons must *escape* from the atmosphere (in fact, this is a very definition of an atmosphere). Hence the photons must be missing in the atmosphere, and thus some elementary atomic transition processes can no longer be balanced, which leads to a non-equilibrium situation.

It is therefore of considerable importance to develop reliable methods which are able to decode the information about a star contained in its spectrum with confidence. Having understood the physics of the problem and being able to carry out detailed numerical simulations will enable us to construct theoretical models of a stellar atmosphere and predict a stellar spectrum. This has important applications in other branches of astrophysics, such as i) derived stellar parameters can be used to verify predictions of the stellar evolution theory; ii) models provide ionizing fluxes for the interstellar medium and nebular models; iii) predicted stellar spectra are basic blocks for population syntheses of stellar clusters, starburst regions, and whole galaxies. Moreover, very hot and massive stars have special significance. They are very bright, and therefore may be studied spectroscopically as individual objects in distant galaxies. Reliable model atmospheres for these stars may therefore yield invaluable independent information about distant galaxies, like chemical composition, and, possibly, reliable distances.

Unlike laboratory physics, where one can change a setup of the experiment in order to examine various aspects of the studied structures separately, we do not have this luxury in astrophysics: we are stuck with the observed spectrum so we should better make a good use of it. This is exactly what the stellar atmosphere theory is doing for almost a century now. Consequently, it is developed to such an extent that it provides an excellent methodological guide for other situations where the radiation has the dual role of a probe and a constituent. Examples of such astronomical objects are the interstellar medium, H II regions, and, in particular, accretion disks.

2 NLTE Model stellar atmospheres

2.1 Background

Model atmospheres which take into account simultaneously departures from local thermodynamic equilibrium (LTE) together with the effects of millions of metal lines – metal line blanketing – are called NLTE line-blanketed models. In the last decade, there has been a considerable effort of several research groups to compute such model atmospheres and to study the effects of NLTE line blanketing upon the atmospheric structure and predicted stellar spectrum. The crucial point was the development of a whole class of methods, generically referred to as Accelerated Lambda Iteration (ALI – for a review, see e.g., Hubeny 1992). The ALI formalism was first applied for constructing model stellar atmospheres by Werner (1986, 1989), and later upgraded to metal line-blanketed models by Dreizler & Werner (1993).

Why do we construct such models? First, we may study the differences between the previous simpler models and the new ones, with the aim to evaluate the differences in deduced basic stellar parameters when these models are used in interpreting observed stellar spectra. Second, from the methodological point of view, one has to proceed step by step. One has to understand well the effect of NLTE metal line blanketing on the atmospheric structure (temperature, ionization stratification, etc.) in a simpler hydrostatic case before one can hope to achieve full understanding of the more complex structure of stellar atmospheres (winds, chromospheres, etc.), or related objects, like accretion disks.

2.2 Method

We have developed a robust numerical scheme, called the hybrid complete linearization/accelerated lambda iteration method (Hubeny & Lanz 1995). The method resembles the traditional complete linearization, however the radiation intensity in most (but not necessarily all) frequencies is not linearized; instead it is treated via the ALI scheme. This method was applied to constructing NLTE line-blanketed model atmospheres for hot, metal-rich DA white dwarfs (Lanz & Hubeny 1995; Lanz et al. 1996b; Barstow, Hubeny, & Holberg 1998; Barstow & Hubeny 1998), O stars (Lanz et al. 1996a), B giants (Hubeny & Lanz 1996), and to hot sdO subdwarfs (Lanz, Hubeny, & Heap 1997).

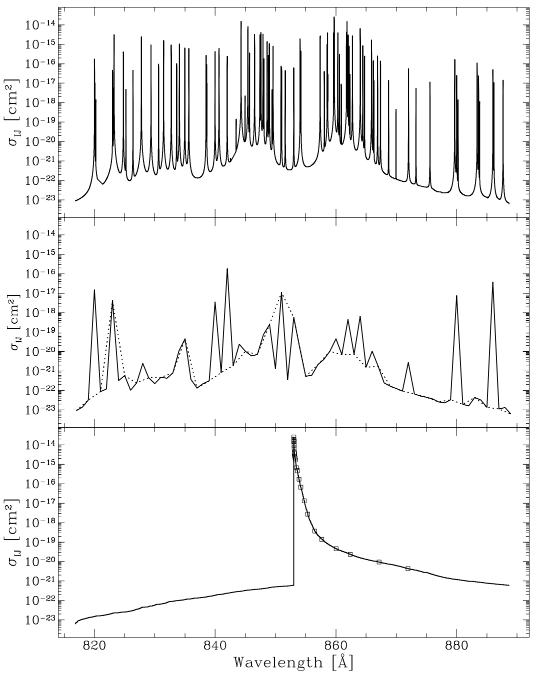

Fig. 1: An illustration of various numerical treatments of a typical superline. Upper panel: the detailed cross-section; Middle panel: the Opacity Sampling representation; Lower panel: the Opacity Distribution Function representation. Small squares indicate the points used to represent this ODF in model atmosphere calculations

Although the ALI-based methods have opened the way to attack the problem of NLTE line blanketing, the enormous complexity of the iron-peak elements (i.e., we have to account for hundreds of energy levels and millions of line transitions per ion) still precludes using direct methods that were successfully used for light elements (H, He, C, N, O, Si, etc.). Statistical methods are therefore necessary. The idea is to avoid dealing with all individual energy levels of complicated metal species. Instead, several states with close enough energies are grouped together to form a so-called "superlevel." The basic assumption is that all individual levels within the same superlevel share the same NLTE departure coefficient; in other words, the individual levels forming a superlevel are in Boltzmann equilibrium with each other. This idea was pioneered by Anderson (1989). The transitions between individual superlevels, called "superlines," are treated by the by means of two possible approaches:

- *Opacity Distribution Functions* (ODF).

The idea is to resample a complicated frequency dependence of the superline cross-section to form a monotonic function of frequency; this function is then represented by a small number of frequency quadrature points (Anderson 1989; Hubeny & Lanz 1995).

- *Opacity Sampling* (OS).
  The idea is a simple Monte Carlo-like sampling of frequency points of the superlevel cross-section (Anderson 1991; Dreizler & Werner 1993). The advantage of this approach is that it can easily treat line blends and overlaps; the disadvantage is that one has to be very careful to choose a sufficiently large number of frequency points, since otherwise the representation may be inaccurate. Indeed, the line cores, which represent the region of maximum opacity, are relatively narrow. Considering too few frequency points may easily lead to missing many important line cores.

These two approaches are illustrated in Fig. 1. We consider the superline between the superlevels 1 and 13 of Hubeny & Lanz (1995) model of Fe III. The detailed cross-section (upper panel) has been computed for some 16 000 internal frequency points. The dotted line in the middle panel represents the Opacity Sampling by 37 (equidistant) wavelength points, while the number of points is doubled for the full line. This shows that unless a large number of frequency points is considered, the OS representation may be quite inaccurate since practically all strong lines are missed. Finally, the lower panel shows the Opacity Distribution Function representation. With 24 points only, we have already a fairly accurate representation of the resampled cross-section to be used in model atmosphere construction.

The strategy for computing line-blanketed model atmospheres is as follows. Hydrogen, helium, and the most important light metals (C, N, O, possibly others) are represented by detailed atomic models, and all the individual lines are treated separately. This involves of the order of a few hundred atomic levels, and up to several thousand lines. The heavy (iron-peak) metals are treated by means of the statistical (ODF or OS) approach. Since the dominant opacity is provided by iron and nickel, we either neglect all the other iron-peak elements, or group all of them together to form an averaged iron-peak element (as suggested first by Anderson 1989).

We have recently implemented the Opacity Sampling approach to TLUSTY. Using TLUSTY, version 198, we are currently calculating (Hubeny & Lanz 2000) a grid of NLTE, fully-blanketed, model atmospheres covering the range of O to early B-type stars ($20000 \le T_{\rm eff} \le 55000$ K, $3.0 \le \log g \le 4.75$) with a solar or 1/5 solar metallicity. The models incorporate over 70,000 NLTE atomic levels of about 30 ions of H, He, C, N, O, Ne, Mg, Si, S, Fe and Ni, which are grouped into about 700 superlevels.

2.3 Some results

To illustrate the overall quality of our NLTE line-blanketed models, we present a sample of the observed UV flux of 10 Lacertae (O9 V), taken by *Goddard High Resolution Spectrograph* (GHRS) aboard the Hubble Space Telescope (HST), together with predictions of our NLTE line-blanketed model with $T_{\rm eff} = 35,000$ K and $\log g = 4$ (see Fig. 2). The rotational velocity is taken as $v \sin i = 25$ km/s. About 9.5 millions of lines of 26 ions of H, He, C, N, O, Si, Fe, and Ni are taken into account in model construction. We assume solar abundances for all elements. The model atmosphere were calculated by TLUSTY and the detailed spectra by the synthetic spectrum program SYNSPEC (Hubeny, Lanz, & Jeffery 1994).

The complete spectrum will be presented elsewhere (Hubeny, Heap, & Lanz, in prep.). Here we show only a small part of the UV spectrum, which is typ-

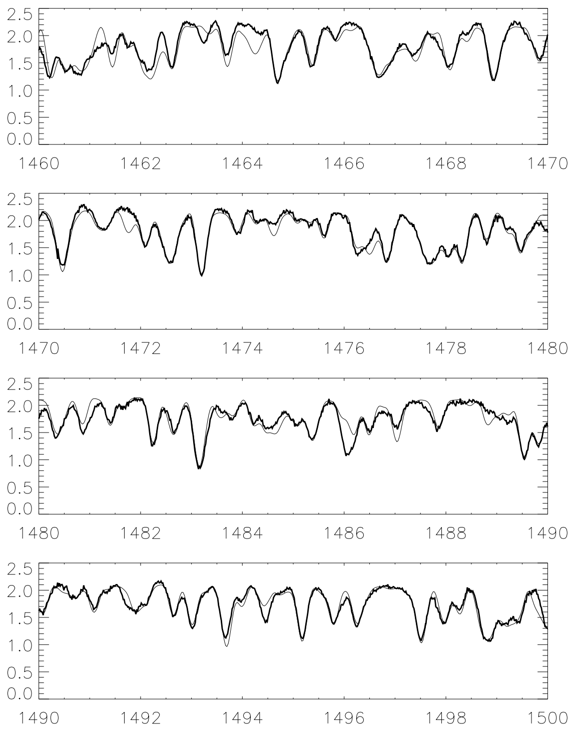

Fig. 2: A comparison of the observed HST/GHRS flux for 10 Lac (heavy line) and the predicted flux from the fully blanketed NLTE model atmosphere with $T_{\rm eff} = 35,000$ K, $\log g = 4$, and $v \sin i = 25$ km/s. The predicted flux is convolved with instrumental broadening with FWHM = 0.06 Å. The abscissa is the wavelength in Å, and the ordinate is the flux in 10^{-9} erg cm^{-2} s^{-1} Å^{-1}.

ical for the quality of the fit in the whole observed region. We see that the agreement of the observed and the predicted spectrum is excellent, which gives us confidence that the non-LTE modeling techniques and the quality of atomic data are sufficiently high to enable us truly detailed spectroscopic studies of hot stars.

3 Quasar Accretion Disk Models

3.1 Background

A black hole that steadily accretes gas from its surroundings at high rates, but below the Eddington limit, should form a geometrically thin accretion disk supported by the residual angular momentum of the gas. For black hole masses in the range $10^8 - 10^9$ $M_\odot$, thought to be typical of bright active galactic nuclei (AGN) and quasars, the peak effective temperature is expected to be around $10^4 - 10^5$ K. This estimate is roughly consistent with the observation that quasar spectra peak in the ultraviolet (the so-called big blue bump), which gave rise to the belief that quasars are indeed powered by accretion onto massive black holes, as first suggested by Shields (1978).

Over the years, many authors have attempted to calculate detailed theoretical spectra of geometrically thin, optically thick accretion disks in order to compare with observation, with varying degrees of sophistication: starting with a local blackbody flux (e.g. Malkan & Sargent 1982); to assuming a local model stellar atmosphere flux (e.g., Kolykhalov & Sunyaev 1984; Sun & Malkan 1989); and finally computing vertical structure together with the radiation field (Laor & Netzer 1989; Ross, Fabian, & Mineshige 1992; Shimura & Takahara 1993, 1995; Coleman 1994; Shields & Coleman 1994; Störzer et al. 1994; Dörrer et al. 1996; Blaes & Agol 1996; and Sincell & Krolik 1998). As reviewed recently by Krolik (1999) and Koratkar & Blaes (1999), these and other models generally suffer from a number of problems when trying to simultaneously explain various features of the observations, in particular optical/ultraviolet continuum spectral shapes, the lack of observed features at the Lyman limit of hydrogen, (e.g., Antonucci, Kinney, & Ford 1989), polarization (Antonucci 1992), the origin of extreme ultraviolet and X-ray emission, and correlated broadband variability (e.g., Alloin et al. 1985). It may be that the resolution of these problems requires a drastic revision of the accretion disk paradigm. Alternatively, it may simply be that the theoretical modeling to date is still too crude to be able to deal satisfactorily with the inherent complexities of the accretion flow. In particular, inclusion of non-LTE effects and detailed opacity sources, Comptonization, and interaction between the disk and X-ray producing regions should all be taken into account.

We have embarked on a long term program to construct detailed model spectra of accretion disks in the axisymmetric, time-steady, thin-disk approximation (Hubeny & Hubeny 1997, 1998; Hubeny et al. 2000) We recognize that there are many possible sources of inconsistencies in the AGN accretion disk modeling. There are essentially two types of problems. First, there are basic physical uncertainties. Among them, the most important is our ignorance of the basic physics of viscous energy dissipation in the AGN disks, so that we are left with a necessity to employ certain *ad hoc* parameters. Although this is certainly a viable approach when nothing else is currently available, we should bear in mind that corresponding models will lack predictive power—we may explain what we see, but we cannot predict it. In any case, when adopting a model based on some chosen set of parameters, one at least has to study carefully the influence of these parameters on the computed model. Second type of problems concerns the degree of approximation used in the actual modeling procedure. Therefore, we study the influence of various approximations, such as departures from LTE, and the completeness of considered opacity and emissivity sources on the computed model.

3.2 Method

We assume a steady–state, thin, rotationally symmetric disk. We define the thin disk by the two conditions, namely *i*) the disk height, $h(R)$, at radial distance R is much smaller than R, i.e., $h(R) \ll R$, and *ii*) all the components of the energy flux vector are negligible to that in the vertical direction, i.e., the direction perpendicular to the disk plane. We also assume the standard disk model, in which the azimuthal velocity is much larger than the radial velocity, and the vertical velocity component is neglected altogether.

The equations for relativistic disk structure were derived by Novikov & Thorne (1973), Page & Thorne (1974), and recently by Riffert & Herold (1996) whose results we are using.

Due to the assumption of thin disk, we may reduce a general 2-D problem of computing disk structure to a set of 1-D problems. The disk is divided into a set of axially symmetric concentric annuli; each annulus behaves as a one-dimensional radiating slab. The vertical structure of a single annulus is computed by solving simultaneously the hydrostatic equilibrium equation, the energy balance equation, the radiative transfer equation, and, since we do not generally assume LTE, the set of statistical equilibrium equations.

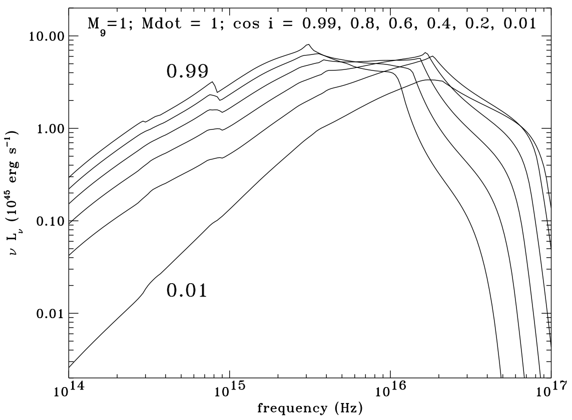

Fig. 3: Integrated spectral energy distribution νL_ν (in erg s^{-1}) for a disk with $M_9 = 1$, $\dot{M} = 1 M_\odot$ yr^{-1}, and for various inclinations.

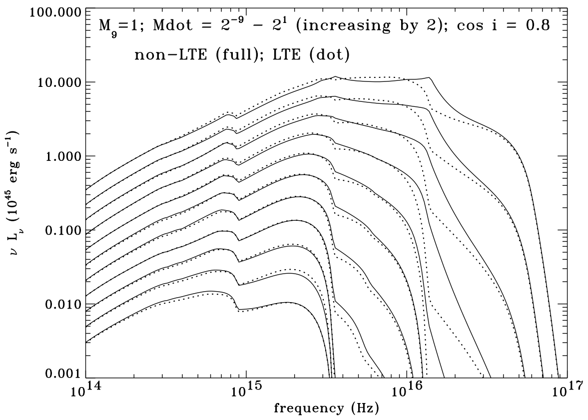

Fig. 4: Integrated spectral energy distribution νL_ν (in erg s^{-1}) for a disk with $M_9 = 1$, $\cos i = 0.8$, and for various values of the mass accretion rate (luminosity), ranging from $L/L_{\rm Edd} = 0.3$ (i.e., $\dot{M} = 2 M_\odot$ yr^{-1}) to $L/L_{\rm Edd} = 3 \times 10^{-4}$ (i.e., $\dot{M} = 2^{-9} M_\odot$ yr^{-1}). Full lines: non-LTE models; dotted lines: LTE models.

Viscosity is the most uncertain physical quantity of the accretion disk modeling. There is no theory that would explain the accretion disk viscosity from first principles. We assume that the viscous stress scales as $t_{r\phi} = \alpha P_{\rm total}$ (Shakura & Sunyaev 1973), where $t_{r\phi}$ and $P_{\rm total}$ are the vertically integrated viscous stress and total vertically-integrated pressure, respectively. The parameter α is an ad hoc, adjustable parameter. However, we are guided by the results of recent studies of the magneto-rotational instability (Balbus & Hawley (1991; Stone et al. 1996) to choose the value of α. We consider two values of α, 0.01 and 0.1, which seems to bracket the range of values following from detailed hydrodynamic simulations

We use the computer program TLUSDISK, which is a derivative of the stellar atmosphere program TLUSTY (Hubeny 1988). The program is based on the hybrid complete-linearization/accelerated lambda iteration (CL/ALI) method (Hubeny & Lanz 1995). A NLTE model of a vertical structure of one annulus of a disk is generally computed in several steps. First, an LTE-gray model is constructed, as described in Hubeny (1990). This serves as the starting solution for the subsequent step, an LTE model, computed by TLUSDISK. This in turn is used as the starting solution for the next step, a NLTE model.

To find the total disk spectrum, we divided the disk into 25-35 radial rings, spaced (roughly) logarithmically. At each ring, after computing the vertical structure, we perform a detailed radiation transfer solution for the Stokes vector as a function of frequency and angle. The spectrum is found by integrating the total emergent intensity over the disk surface using our relativistic transfer function code (Agol 1997). The transfer function computes the trajectories of photons from infinity to the disk plane, finding the emitted radius, redshift, and intensity at each image position at infinity for a given observation angle (Cunningham 1975). So far, we have neglected the effects of radiation which returns to the accretion disk, although we plan to include this effect in future studies.

3.3 Some results

We have constructed (Hubeny et al. 2000) a grid of models for a black hole spin of $a/M = 0$ (Schwarzschild black hole), and 0.998 (maximum rotation Kerr black hole), luminosities between $3 \times 10^{-4} L_{\rm Edd}$ and $0.3 L_{\rm Edd}$, and black hole masses between $M_9 \equiv 10^{-9} M/M_\odot = 0.125$ to $M_9 = 32$.

We first present integrated spectra for a disk of given mass and luminosity, $M_9 = 1$, $L/L_{\rm Edd} = 0.15$ (i.e. $\dot{M} = 1 M_\odot$ yr^{-1}), and for various values of the inclination angle i, ranging from $\cos i = 0.99$ (i.e., the disk seen almost face-on), to $\cos i = 0.01$ (the disk seen almost edge-on) – Fig. 3. We can clearly see the impact of relativistic boosting and aberration: the flux at the highest frequencies (radiated where the disk is most relativistic) is boosted strongly for viewing angles near the disk plane. Also for such viewing angles, gravitational light bending counteracts the classical, Newtonian projection effect.

Next, we present the integrated spectra for one value of inclination. We chose $\cos i = 0.8$ (i.e., $i \approx 37°$), which is a value relatively close to face-on, and which thus may serve as a typical value for type 1 AGN and QSO's based on unification arguments (e.g., Krolik 1999). Figure 4 shows the integrated spectra for one particular value of the black

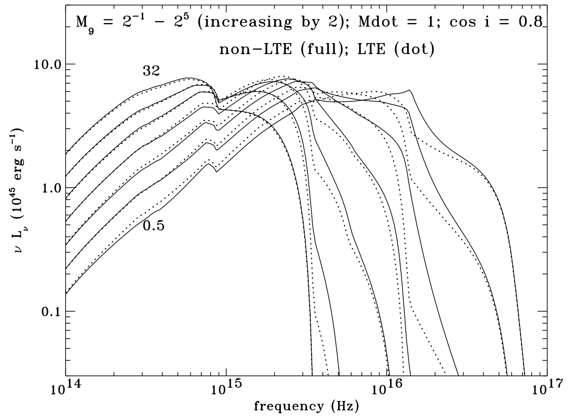

Fig. 5: Integrated spectral energy distribution νL_ν (in erg s^{-1}) for a disk with $\dot{M} = 1 M_\odot$ yr^{-1}, $\cos i = 0.8$, and for various values of the black hole mass, M_9, ranging from $M_9 = 32$ to 0.5.

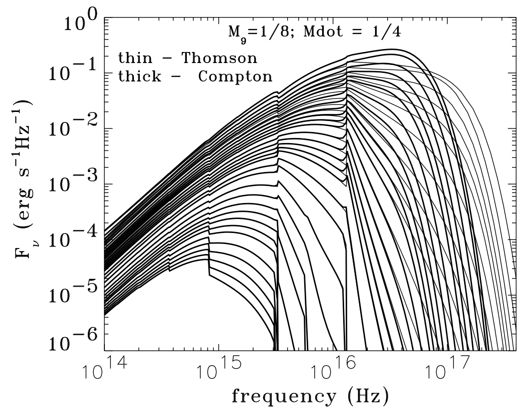

Fig. 6: Local emergent flux for the individual annuli. From top to bottom, the curves correspond to radii R/R_g = 1.5, 2, 2.5, 3, 3.5, 4, 5, 6, 7, 8, 9, 10, 12, 14, 16, 18, 20, 25, 30, 40, 50, 60, 70, 80, 90, 100, 120, 140, 160, 180, and 200. Thin lines represent the models from Hubeny et al. (2000) computed without Comptonization, and thick lines represent the models with Comptonization.

hole mass, $M_9 = 1$, and for various luminosities (mass accretion rates). Full lines display non-LTE models, while the dotted lines display LTE model predictions. The spectral energy distribution is hardest for the largest luminosity. The non-LTE effects are most important in the He II Lyman continuum ($\nu > 1.36 \times 10^{16}$ Hz), and also for predicting the detailed shape of the hydrogen Lyman edge for intermediate and low luminosities.

In Figure 5 we display the sequence of predicted spectra for models with a fixed mass accretion rate (i.e., total luminosity) and varying black hole mass. The energy distribution is progressively shifted towards more energetic photons for lower masses, because disks around less massive holes have smaller radiating surface areas. The non-LTE effects are important for all disks; for hotter ones the largest departures from LTE are seen in the He II Lyman continuum, and in cooler ones in the hydrogen Lyman continuum.

We have recently implemented the effects of Comptonization, i.e. the effects of non-coherent electron scattering. Comptonization grows in importance as the central mass decreases and the central temperature rises: it has little effect when $M > 10^8 M_\odot$. It generally produces an increase in temperature with height in the uppermost layers of hot atmospheres. Compared to models with coherent electron scattering, Comptonized models have enhanced extreme ultraviolet/soft X-ray emission, but they also have a more sharply declining spectrum at high frequencies. Comptonization also smears the hydrogen and the He II Lyman edges.

To illustrate this behavior, we present the emergent flux for the individual annuli for the disk around a black hole with $M = (1/8) \times 10^9$ M$_\odot$ and mass accretion rate $\dot{M}$ = 1/4 M$_\odot$/yr (i.e. with luminosity $L \approx 0.3\,\mathrm{L_{Edd}}$). Figure 6 displays a comparison between the model without (thin lines) and with (heavy lines) Comptonization for the individual annuli. Comptonization in hot annuli leads to the well-known increase of the flux in the EUV and the soft X-ray region ($\nu < 10^{17}$ s^{-1}). For larger frequencies, the flux drops fast, so that the flux for the Comptonized model is lower than the flux for the original, Thomson-scattering, model.

Finally, we present an example of a comparison of observed and theoretical spectra of an actual quasar. We take a high-redshift quasar Q0302-003 ($z = 3.29$), which was observed by the *Space Telescope Imaging Spectrograph* (STIS) – Heap et al. (2000). Figure 7 displays the observed continuum flux of Q 0302-003 transformed to the quasar rest frame, using $z = 3.29$, and the standard cosmology with H_0 = 65 km s^{-1} Mpc^{-1}, Ω_0 = 0.2, and Λ = 0, (i.e. q_0 = 0.1). The observed spectrum is taken from Sargent, Steidel, & Boksenberg (1989), and from the STIS data. The best fit was obtained for a disk with the black hole mass $M = 8 \times 10^9$ $M_\odot$ and the mass accretion rate $\dot{M}$ = 10 $M_\odot$ yr^{-1}, seen almost face-on, with an inclination $\cos i = 0.99$.

4 Conclusions

We have shown that the recent progress in the fast and ingenious numerical methods, namely those based on the Accelerated Lambda Iteration, has led to an enormous progress in the degree of realism in computed model atmospheres. We are now able to compute fully blanketed non-LTE model atmospheres, taking into account literally tens of millions of spectral lines in NLTE. What was a dream only a decade ago is now becoming a reality.

On the quasar side, the results presented here do not indicate any fatal flaw of the AGN accretion disk paradigm. In contrast, they show that one of the previous critical arguments against the accretion disk paradigm, the magnitude of the Lyman jump, essentially disappears when increasing a degree of realism of the modeling procedure by relaxing previous simplifying approximations, in particular the local thermodynamic equilibrium and a simplified vertical disk structure. However, this study has concentrated on only one aspect of the problem, the spectral energy distribution in the optical, UV, and EUV region. Many questions, such as the overall spectral energy distribution of the whole disk, the effects of external irradiation, the continuum polarization, etc., remain to be explored in the future.

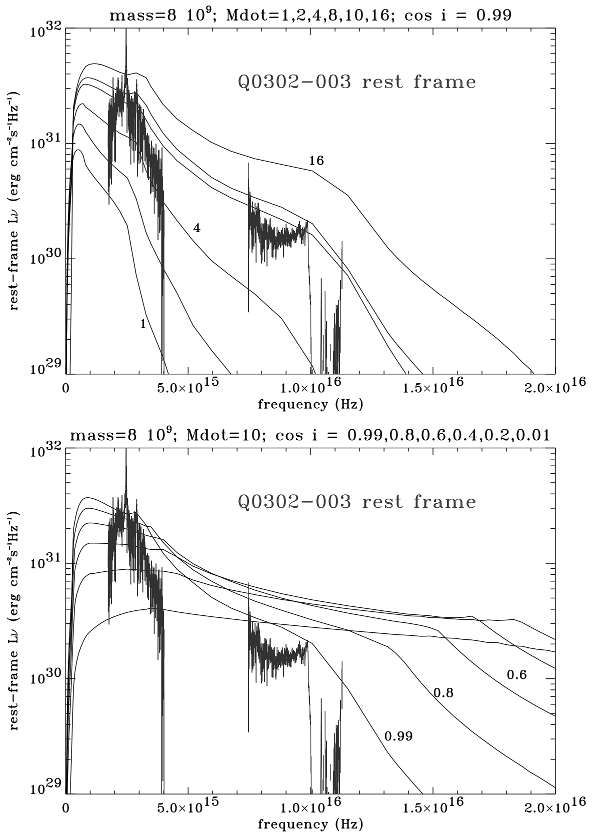

Fig. 7: A comparison of the observed continuum flux of Q 0302-003 transformed to the quasar rest frame, using $z = 3.29$, $H_0 = 65$ km s^{-1} Mpc^{-1}, and $q_0 = 0.1$. Upper panel: theoretical models of a bare accretion disk around a supermassive, Kerr black hole with the black hole mass $M = 8 \times 10^9\ M_\odot$ and the mass accretion rates $\dot{M} = 1, 2, 4, 8, 10,$ and $16\ M_\odot\,\mathrm{yr}^{-1}$. The lower panel: model for $M = 8 \times 10^9\ M_\odot$ and $\dot{M} = 10\ M_\odot\,\mathrm{yr}^{-1}$, for various disk inclinations. All the models assume the maximum stable rotation of the black hole, $(a/M) = 0.998$.

References

Agol, E. 1997, Ph.D. thesis, Univ. California, Santa Barbara

Alloin, D., Pelat, D., Phillips, M., & Whittle, M. 1985, ApJ 288, 205

Anderson, L. S. 1989, ApJ 339, 588

Anderson, L. S. 1991: in Stellar Atmospheres: Beyond Classical Models, ed. by ed. L. Crivellari, I. Hubeny, & D.G.Hummer, NATO ASI Series C 341, Kluwer, Dordrecht, 29

Antonucci, R.R.J. 1992, in Testing the AGN Paradigm, ed. by S.S. Holt, S.G. Neff, & C.M. Urry, 486

Antonucci, R., Kinney, A. L., & Ford, H. C. 1989, ApJ 342, 64

Auer L.H., & Mihalas D. 1969, ApJ 158, 641

Balbus, S.A., & Hawley, J.F. 1991, ApJ 376, 214

Barstow, M.A., & Hubeny, I. 1999, MNRAS 299, 379

Barstow, M.A., Hubeny, I., & Holberg, J.B. 1999, MNRAS 299, 520

Blaes, O., & Agol, E. 1996, ApJ 469, L41

Coleman, H.H. 1994, PhD thesis, Univ. of Texas

Cunningham, C. T. 1975, ApJ 202, 788

Dörrer, T., Riffert, H., Staubert, R., & Ruder, H. 1996, A&A 311, 69

Dreizler, S., & Werner, K. 1993, A&A 278, 199.

Heap, S.R., Williger, G.M., Smette, A., Hubeny, I., Sahu, M.S., Jenkins, E.B., Tripp, T.M., & Winkler, J.N. 2000, ApJ 534, 69

Hubeny, I. 1988, Comp. Phys. Comm. 52, 103

Hubeny, I. 1990, ApJ 351, 632

Hubeny, I. 1992, in The Atmospheres of Early-Type Stars, ed. by U. Heber & C.S. Jeffery, Lecture Notes in Phys. 401, Berlin: Springer, 377

Hubeny, I., & Hubeny, V. 1997, ApJ 484, L37

Hubeny, I., & Hubeny, V. 1998, ApJ 505, 558

Hubeny, I., & Lanz, T. 1992, A&A 262, 501

Hubeny, I., & Lanz, T. 1995, ApJ 439, 875

Hubeny, I., & Lanz, T. 1996, in Astrophysics in the Extreme Ultraviolet, ed. by S. Bowyer and R.F. Malina, Kluwer, Dordrecht, 381

Hubeny, I., & Lanz, T. 2000, BAAS 197, 78.12

Hubeny, I., Lanz, T., & Jeffery, C. S. 1994, in Newsletter on Analysis of Astronomical Spectra No. 20, Ed. C.S. Jeffery, St Andrews Univ., 30

Hubeny, I., Agol, E., Blaes, O., & Krolik, J. H. 2000, ApJ 533, 710

Kolykhalov, P. I., & Sunyaev, R. A. 1984, Adv. Space Res. 3, 249

Koratkar, A., & Blaes, O. 1999, PASP 111, 1

Koratkar, A. P., Kinney, A. L., & Bohlin, R. C. 1992, ApJ 400, 435

Krolik, J. H. 1999, Active Galactic Nucle, Princeton Univ. Press, Princeton

Lanz, T., & Hubeny, I. 1995, ApJ 439, 905
Lanz, T., Hubeny, I., & Heap, S. R. 1997, ApJ 485, 843
Lanz, T., de Koter, A., Hubeny, I., & Heap, S. R. 1996a, ApJ 465, 359
Lanz, T., Barstow, M.A., Hubeny, I., & Holberg, J. B. 1996b, ApJ 473, 1089
Laor, A., & Netzer, H. 1989, MNRAS 238, 897
Malkan, M. A., & Sargent, W.L.W. 1982, ApJ 254, 22
Novikov, I.D., & Thorne, K.S. 1973, in Black Hole Astrophysics, ed. by De Witt, C., & De Witt, B., Gordon and Breach, New York, 343
Page, D., & Thorne, K. S. 1974, ApJ 191, 499
Riffert, H., & Herold, H. 1995, ApJ 450, 508
Ross, R. R., Fabian, A. C., & Mineshige, S. 1992, MNRAS 258, 189
Sargent, W.L.W., Steidel, C.C., & Boksenberg, A. 1989, ApJS 69,703
Shakura, N. I., & Sunyaev, R. A. 1973, A&A 24 337
Shields, G. 1978, Nature 272, 706
Shields, G.A., & Coleman, H.H. 1994, in Theory of Accretion Disks - 2, ed. by W.J. Duschl et al., Kluwer, Dordrecht, 223
Shimura, T., & Takahara, F. 1993, ApJ 419, 78
Shimura, T., & Takahara, F. 1995, ApJ 440, 610
Sincell, M. W., & Krolik, J. H. 1998, ApJ 496, 737
Stone, J.M., Hawley, J.F., Balbus, S.A., & Gammie, C.F. 1996, ApJ 463, 656
Störzer, H., Hauschildt, P. H., & Allard, F. 1994, ApJ 437, L91
Sun, W.-H., & Malkan, M. A. 1989, ApJ 346, 68
Werner, K. 1986, A&A 161, 177
Werner, K. 1989, A&A 226, 265